

One-dimensional Josephson junction arrays: Lifting the Coulomb blockade by depinning

Nicolas Vogt,¹ Roland Schäfer,² Hannes Rotzinger,³ Wanyin Cui,^{3,2}
Andreas Fiebig,^{3,2} Alexander Shnirman,^{1,4} and Alexey V. Ustinov³

¹*Institut für Theorie der Kondensierten Materie,*

Karlsruhe Institute of Technology, D-76128 Karlsruhe, Germany

²*Institut für Festkörperphysik, Karlsruhe Institute of Technology, D-76021 Karlsruhe, Germany*

³*Physikalisches Institut, Karlsruhe Institute of Technology, D-76128 Karlsruhe, Germany*

⁴*L. D. Landau Institute for Theoretical Physics RAS, Kosygina street 2, 119334 Moscow, Russia*

(Dated: March 2, 2022)

Experiments with one-dimensional arrays of Josephson junctions in the regime of dominating charging energy show that the Coulomb blockade is lifted at the threshold voltage, which is proportional to the array's length and depends strongly on the Josephson energy. We explain this behavior as de-pinning of the Cooper-pair-charge-density by the applied voltage. We assume strong charge disorder and argue that physics around the de-pinning point is governed by a disordered sine-Gordon-like model. This allows us to employ the well-known theory of charge density wave de-pinning. Our model is in good agreement with the experimental data.

PACS numbers: 74.81.Fa, 74.50.+r, 73.23.Hk

Keywords: Josephson-Junction-Arrays, Depinning

One-dimensional Josephson arrays show a diverse range of transport regimes. In the regime of dominating Josephson energy, which attracts a continued experimental interest¹⁻³, they are highly conducting. In the regime of Josephson energy smaller or comparable to the charging energy, one-dimensional Josephson arrays show insulating (Coulomb blockade) behavior with activated transport⁴. Above a certain threshold value of the bias voltage, finite current appears even at zero temperature in the insulating regime. Initially, this switching was interpreted in terms of propagation onset of charge solitons⁵⁻⁷, i.e., the energy one has to pay in order to push one soliton into the array. However, further experiments showed that the threshold voltage is proportional to the array length and depends strongly on the value of the Josephson energy^{1,8}. Here we interpret the experimentally found behavior as de-pinning in presence of strong charge disorder⁹.

We argue that the system is described by a model similar to a disordered sine-Gordon model. The only difference is the fact that, instead of the usual cosine potential, we have another periodic function, the lowest Bloch band energy, which depends strongly on the Josephson energy. It is this dependence which gives rise to the dependence of the switching voltage on the Josephson energy. Previously, similar models were derived^{1,6-8,10} using an additional phenomenological inductance in each cell of the array, which provided the necessary mass term. In Ref. 11 it was shown, that a mass term is generated in the adiabatic regime due to the Bloch inductance¹² and the phenomenological inductance is not needed. We argue that the adiabatic mechanism is sufficient to describe the system prior and at the de-pinning point.

For this work, a series of experiments has been performed on a set of three Josephson junction chains. The three arrays have been fabricated in parallel on the

same silicon substrate covered by an insulating thermally grown SiO₂ layer. The individual cells of the array are implemented as SQUID loops, similarly to earlier experiments^{1,7}. The two tunnel junctions in each SQUID are equivalent to a single junction with an effective Josephson energy $E_J(\Phi)$ tunable by the magnetic flux Φ penetrating the loop area A . That gives $E_J(\Phi) = E_J^m |\cos(\pi\Phi/\Phi_0)|$, where E_J^m is twice the Josephson energy of one bare Josephson junction of the SQUID and $\Phi_0 = h/2e$ is the magnetic flux quantum.

The set of samples contains nominally identical arrays (labeled A255, B255, and C255) comprising each 255 SQUIDs. These arrays had very similar resistances. Nevertheless, slight variations in the junction parameters are reflected in the I - V characteristics¹³.

The experiments have been performed in a ³He/⁴He dilution refrigerator at 20 mK temperature. A scanning electron microscope (SEM) picture of a section of one of the arrays is shown in the left inset of Fig. 1. All electrical connections to the samples are carefully filtered by a combination of lumped-element low pass RC -filters and metal powder filters covering a bandwidth of 10 kHz. I/V characteristics are measured by ramping the applied bias voltage and recording the resulting current with a homemade transimpedance amplifier. A typical I/V characteristic is shown in Fig. 1, where the blue curve is recorded while the bias voltage is ramped up and the red curve represents the behavior for decreasing bias. In all cases, the current vanishes below a certain threshold; for the horizontal branch, no current can be detected within the resolution of our current measurement which is of the order of 50 fA¹³. At a value $V_{sw}(\Phi)$, the chain switches to a conducting state; the current after the switching is flux dependent and has a magnitude of at least several pA. Retrapping to the $I = 0$ branch happens at a much lower voltage $V_{rt} < V_{sw}$. In this paper, we focus on

the magnitude and the flux dependence of the switching voltage $V_{sw}(\Phi)$. We expect V_{sw} to be primarily a function of $E_J(\Phi)$. Thus, $V_{sw}(\Phi)$ is a periodic function in Φ with a period of Φ_0 . Experimentally, we observe the period (measured in units of the external magnetic field) to be of order $B_{ext} = 6.9 \text{ mT}$, corresponding to an area of $\Phi_0/6.9 \text{ mT} = 0.3 \mu\text{m}^2$. This agrees well with the total area per SQUID loop, $A_{\text{SQUID}} = 1.6 \mu\text{m} \cdot 200 \text{ nm}$ defined by the sample layout.

The rate by which the bias voltage at the sample can be changed is limited by the bandwidth of the connecting leads (10 kHz). In some cases we recorded histograms for the switching voltage. The method used to record switching histograms is detailed in Appendix F. A typical example is shown as the middle inset in Fig. 1. The distribution of switching events turns out to be rather broad (e.g. $\sim 1 \text{ mV}$ for sample B255). However, this measurements confirmed that the switching voltage as extracted from single I/V characteristics is close to the mean of the histograms with a dispersion reflecting the width of the distribution.

The system is modeled as an array of superconducting islands (squares in the inset of Fig. 1) connected by Josephson junctions (crosses in the inset of Fig. 1). The junctions are characterized by the effective Josephson energy E_J (controlled by the magnetic field) and by the effective capacitance $C_J \approx 2C_1$ (C_1 being the capacitance of each of the SQUID junctions), which determines the (single electron) charging energy scale $E_C = e^2/2C_J$.

Based on the area of the Al/AlO_x/Al tunnel junctions deduced from SEM micrographs we estimate that the average capacitance of the junctions is $C_J \approx 1 \text{ fF}$. Due to variations in the areas of the tunnel junctions the values of C_J are not necessarily constant along the array.

Screening, dominated by two ground planes running alongside of the array is modeled by attributing to each island a capacitance to the ground C_0 (see inset of Fig. 1). This gives the screening length $\Lambda \equiv \sqrt{C_J/C_0}$ and introduces yet another charging energy scale $E_{C0} \equiv e^2/2C_0 = \Lambda^2 E_C$. We estimate $5 \text{ aF} < C_0 < 20 \text{ aF}$.

In our theory we include disorder in the gate (frustration) charge $2ef_k$ on each superconducting island. The Hamiltonian then reads $H = H_C + H_J$, where

$$H_C = \frac{(2e)^2}{2} \sum_{k,q} (n_k - f_k) [C^{-1}]_{kq} (n_q - f_q) \quad (1)$$

and $H_J = -\sum_k E_J \cos(\theta_k - \theta_{k+1})$. Here n_i is the number of Cooper-pairs on island k , and $[n_k, \exp(i\theta_q)] = \delta_{k,q}$. The capacitance matrix is given by $C_{kq} = (2C_J + C_0) \delta_{k,q} - C_J (\delta_{k-1,q} + \delta_{k+1,q})$. In the regime $C_J \gg C_0$, i.e., $\Lambda \gg 1$, one obtains $[C^{-1}]_{kq} \approx C_J^{-1} (\Lambda/2) \exp[-|k - q|/\Lambda]$. Arrays with charge disorder in the limit $C_J \gg C_0$ have been considered long ago (see, e.g.,^{14,15}). The onset of charge transport was calculated purely from the analysis of the stability of charge configurations. The crucial difference in our work is the strong renormalization of the disorder potential in the regime

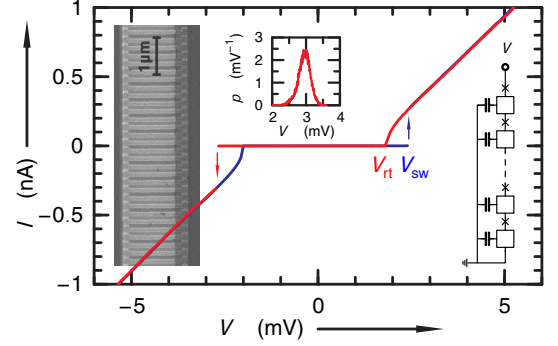


FIG. 1. (color online) Hysteretic I - V characteristics of array B255 measured for increasing voltages (blue) and decreasing voltages (red) at $\Phi = 0$. The left inset shows an SEM micrograph of the Josephson junction array; the right inset is a schematic representation of the array. The middle inset displays the probability density function of V_{sw} .

$E_J \sim E_C$.

The model introduced above was considered (without disorder) in Refs. 16 and 17 in the regime $E_J \gg E_C$ and also in Ref. 18. It was demonstrated that in the thermodynamic limit the system undergoes a Beresinskii-Kosterlitz-Thouless quantum phase transition and is an insulator for $K < 2$, where $K \equiv \pi \sqrt{E_J/(8E_{C0})} = \pi \Lambda^{-1} \sqrt{E_J/(8E_C)}$. Note, that due to $\Lambda \gg 1$ the regime $K \ll 1$ is compatible with $E_J \gg E_C$.

As realized in Refs. 16 and 17, in the regime $\Lambda \gg 1$ it is preferable to use the phase and charge variables of the junctions rather than those of the islands. Thus we introduce the phase drops on the Josephson junctions $\phi_k \equiv \theta_k - \theta_{k+1}$ and their conjugate charge variables $m_k \equiv \sum_{p=1}^k n_p$. We express H_C in terms of m_k and after some algebra conclude that H_C can be obtained by minimizing

$$H_C\{Q\} = \sum_{k=1}^N \left[\frac{(2em_k - F_k - Q_k)^2}{2C_J} + \frac{(Q_k - Q_{k+1})^2}{2C_0} \right] \quad (2)$$

with respect to continuous charge variables Q_k . That is $H_C = \min_Q [H_C\{Q\}]$. Here $F_k \equiv 2e \sum_{p=1}^k f_p$ is the accumulated random gate charge. The quasi-charges Q_k are well known in the theory of Coulomb blockade and appear naturally in the theories including a phenomenological inductance^{6,10}. Their electrostatic meaning and the derivation with inductances is explained in Appendix A.

The introduction of Q_k is equivalent to a Hubbard-Stratonovich transformation in the sense that, e.g., the real time (Keldysh) partition function can be obtained as $Z = \mathcal{N} \int \prod_k DQ_k Dm_k D\phi_k e^{i \int dt [\sum_k m_k \dot{\phi}_k - H_C\{Q\} - H_J]}$, where \mathcal{N} is a normalization factor. For a given path of the quasi-charges $Q_k(t)$ the (m_k, ϕ_k) -dependent part of the Hamiltonian $H_C\{Q\} + H_J$ separates into Hamiltonians of independent Josephson junctions biased each

by charge $Q_k + F_k$, i.e.,

$$H_k = \frac{1}{2C_J} (2em_k - Q_k - F_k)^2 - E_J \cos \phi_k. \quad (3)$$

To obtain the effective quasi-charge theory we integrate out the discrete charge degrees of freedom m_k, ϕ_k . At temperatures much lower than the band gap of (3), i.e., the Q -dependent energy splitting between the ground and the first excited states of (3), and close enough to equilibrium it should be sufficient¹⁰ to consider only adiabatic paths $Q_k(t)$ as was done in Ref. 11. These are paths that do not induce Landau-Zener transitions between the energy bands of (3). Generalizing the derivation of Ref. 11 to the regime of charge disorder and defining $Q_k^F \equiv Q_k + F_k$ we obtain the following effective Lagrangian

$$\mathcal{L} = \sum_k \left[\frac{L_B(Q_k^F) \dot{Q}_k^2}{2} - \frac{(Q_k - Q_{k+1})^2}{2C_0} - U[Q_k^F] \right]. \quad (4)$$

Here $L_B(Q)$ is the Bloch inductance^{11,12} whereas $U[Q]$ is the zeroth Bloch band energy (Q -dependent ground state energy of (3)). Thus, the mass term $\propto L_B$ is generated and the phenomenological inductance used in^{6,10} is not necessary. In this paper, we are interested in depinning and approach this transition from the non-dynamical pinned side, where fast changes in the quasi-charge are naturally suppressed. Thus, we argue that the description in terms of slow adiabatic paths $Q_k(t)$ is applicable, at least for not very small values of E_J . This assumption will be checked for self-consistency below.

Our central idea here is that in the regime $E_J \sim E_C$ and $\Lambda \gg 1$ the model (4) is still applicable whereas the pinning potential is strong and varies significantly with varying $E_J(\Phi)$. This explains the strong dependence of the switching voltage on Φ . The idea of classical charge pinning in Josephson arrays was first proposed by Gumarie and Tsvelik¹⁰. There, the classical regime $K \ll 1$ was achieved by introducing a phenomenological large inductance⁶. Our main achievement here is in showing that Bloch inductance is sufficient to render the pinning regime.

To describe the onset of transport (depinning) it is sufficient to focus on the potential energy part of (4). In the continuum limit justified by large Λ , we obtain the following well established continuum model for CDW-depinning⁹

$$H_C = \int dx \left[\frac{(\partial_x Q(x))^2}{2C_0} + U[Q(x) + F(x)] - E Q(x) \right], \quad (5)$$

where the spatial coordinate x is measured in units of the array lattice constant. Here $E \equiv V/N$ is the homogeneous depinning force (electric field). In Appendix C we discuss the case of the bias voltage applied at the edge.

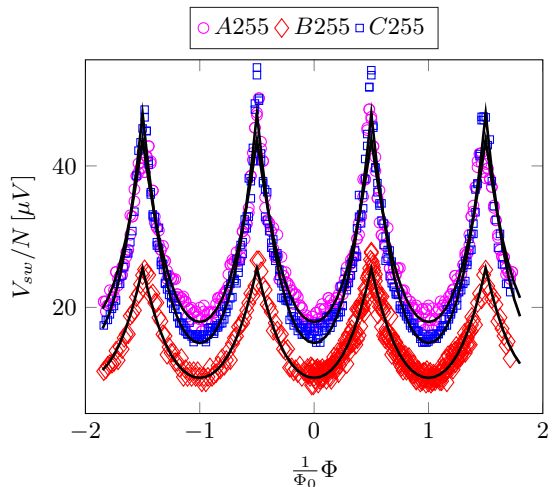


FIG. 2. (color online) The switching voltage normalized to the array length N as a function of the magnetic flux Φ for three arrays of length 255. Solid lines are fitted functions, circles show experimental data.

We assume a strong (maximal) charge disorder, i.e., the gate charges $2ef_k$ being homogeneously distributed in an interval of length $2e$ or larger. This is equivalent to a homogeneous distribution of F_k between $-e$ and e and statistical independence of F_k and F_q for $k \neq q$. Indeed, the disorder charge F_k is effectively limited to the interval $[-e, e]$ as any deviation thereof is compensated by adjusting the number of Cooper-pairs on the islands.

As discussed in detail in the literature (for review see Ref. 9), the critical value of the depinning force is determined by the competition between the disorder pinning potential and the elastic energy. The two become comparable at the so called Larkin length N_L (a.k.a. Fukuyama-Lee or Imry-Ma length)¹⁹⁻²¹ and at $E_p \approx e(C_0 N_L^2)^{-1}$ the charge is depinned²².

The Larkin length is calculated²¹ using the pinning strength R of the effective potential $U(Q)$,

$$R = \max_{Q \in [-e, e]} [U(Q)] - \min_{Q \in [-e, e]} [U(Q)]. \quad (6)$$

One obtains for the Larkin length²¹

$$N_L \approx 3^{-2/3} \Lambda^{4/3} \tilde{R}^{-1/3}, \quad (7)$$

where $\tilde{R}[E_J(\Phi)/E_C] \equiv \frac{1}{16E_C^2} R^2$. The dependence of \tilde{R} on the dimensionless parameter $E_J(\Phi)/E_C$ is obtained numerically (see Appendix D).

Thus, we obtain the following estimate for the switching voltage

$$V_{sw} = NE_p \approx \frac{2NE_C}{e} 3^{4/3} \Lambda^{-2/3} \tilde{R}^{2/3}. \quad (8)$$

This expression is valid as long as the Larkin length is much shorter than the array length, $N_L \ll N$.

We use Eq. (8) to fit the experimental data for arrays A255, B255, and C255 (see Fig. 2). From the device

fabrication one can expect the value of the ground capacitance C_0 to vary only to a small degree between the samples. At the same time an exact value for C_0 can not be determined experimentally. The other parameters of the array islands, C_J and E_J^m , can vary between different samples and also between different islands of the same sample due to imperfections in the junctions. We use the obtained fitting parameters to express the effective C_J and E_J^m in terms of the undetermined C_0 and give the values corresponding to either $C_0 = 5\text{aF}$ or $C_0 = 20\text{aF}$ (Tab. I). We obtain values of C_J and E_J^m that are comparable with the ones expected from geometrical estimates. (Given the uncertainty of the numerical coefficients in (8), some deviations should be expected.) As the Larkin length N_L depends on E_J , we only provide the maximal value N_L^{max} , achieved at $\Phi = 0$, where $E_J = E_J^m$, and the minimal value N_L^{min} , achieved at $\Phi = \Phi_0/2$, where $E_J \approx 0$. The depinning approach is applicable since $N_L < N$.

array	A255	B255	C255
N	255	255	255
$C_J \Lambda^{\frac{2}{3}} = C_J^{\frac{4}{3}} C_0^{-\frac{1}{3}}$	$2.5 \pm 0.01 \text{ fF}$	$4.27 \pm 0.03 \text{ fF}$	$2.3 \pm 0.01 \text{ fF}$
E_J^m / E_C	1.27 ± 0.02	1.33 ± 0.02	1.63 ± 0.02
C_J ($C_0 \approx 5\text{aF}$)	0.53 fF	0.79 fF	0.5 fF
Λ ($C_0 \approx 5\text{aF}$)	10.3	12.6	10
E_J^m ($C_0 \approx 5\text{aF}$)	$192 \mu\text{eV}$	$134 \mu\text{eV}$	$262 \mu\text{eV}$
$N_L^{\text{min/max}}$ ($C_0 \approx 5\text{aF}$)	[27, 42]	[35, 56]	[26, 46]
C_J ($C_0 \approx 20\text{aF}$)	0.75 fF	1.12 fF	0.7 fF
Λ ($C_0 \approx 20\text{aF}$)	6.1	7.5	6.0
E_J^m ($C_0 \approx 20\text{aF}$)	$136 \mu\text{eV}$	$95 \mu\text{eV}$	$186 \mu\text{eV}$
$N_L^{\text{min/max}}$ ($C_0 \approx 20\text{aF}$)	[13, 21]	[18, 28]	[13, 23]

TABLE I. The experimental estimates and fitted values for Josephson junction arrays A255, B255, and C255.

When comparing to other previously explored models we notice the difference between the physics we describe here and the de-pinning of a single charge soliton in a disordered array. The latter case was analyzed within the disordered sine-Gordon model²³. It was shown that the depinning critical force grows with the soliton length Λ . In our case, however, the depinning transition is a collective phenomenon in the whole array. At the transition point the array contains, on average, one extra charge of $2e$ per Larkin length, $N_L \propto \Lambda^{4/3} \tilde{R}^{-1/3}$. The longer is Λ , the fewer charges are pinned and the easier is the depinning, $E_p \propto \Lambda^{-\frac{2}{3}} \tilde{R}^{2/3}$. As mentioned above, models of transport onset that rely on the creation of a propagating soliton⁷ can not explain the linear dependence of V_{sw} on N , observed in experiments.

We, finally, check the consistency of our adiabatic assumption. Clearly, it is well justified if $E_J \gg E_C$ and it must break down if $E_J \ll E_C$. To get a more precise criterium, we assume $E_J \approx E_C$ and estimate the typical

oscillation (pinning) frequency of a domain of length N_L with a rigid quasi-charge Q . We obtain $\omega_p \sim \sqrt{\frac{2E_J E_C}{N_L}}$ (cf.^{10,24-26}). We compare this with the plasma frequency $\sqrt{8E_J E_C}$, which in this regime is also of the order of the critical Landau-Zener frequency. We conclude that, parametrically, for $N_L \rightarrow \infty$, e.g., for $\Lambda \rightarrow \infty$, the adiabatic assumption is well justified. More precise estimates show that, for our arrays, the adiabatic assumption is valid except for a narrow domain of Φ around $\Phi_0/2$ where $E_J(\Phi) \ll E_C$.

In this paper we have compared the experimentally measured magnetic flux dependence of the switching voltage of an insulating (Coulomb blockaded) SQUID-array with our theoretical predictions based on a sine-Gordon-like model for a continuous quasi-charge field. Based on Ref. 11 we argue that this model can be applied without introducing artificial large inductances^{1,6,7,10}. We employ the connection to the theory of charge density wave depinning, first pointed out in Ref. 10, to theoretically analyze the switching voltage and fit the experimental data. We find that the breakdown of the insulating state in Josephson junction arrays is a collective depinning effect, similar to that of depinning of charge density waves, vortices in type II superconductors etc. The switching behavior of Josephson junction arrays can therefore be linked to a rich research area of physics. We think this could be particularly interesting as Josephson junction arrays are artificially fabricated and could possibly help us to study depinning physics in the limit of very short systems or at the crossover from discrete systems to the continuum limit. Transport well above the switching voltage remains the subject of continuing investigations²⁷. It will be interesting to match this transport regime with the depinning physics analyzed in this paper.

ACKNOWLEDGMENTS

We thank A.D. Mirlin, J.H. Cole, B. Kiebig, D.G. Polyakov, S.V. Syzranov, and T. Giamarchi for helpful discussions of the subject. The theory analysis was funded by the Russian Science Foundation under Grant No. 14-42-00044.

Appendix A: Array with inductances

The introduction of inductances L_0 into the model (see Fig. 3) necessitates a description in terms of continuous as well as discrete charge variables. The discrete ones are the overall charges $2en_i$ of the islands. The continuous ones are the charges q_i on the junction capacitances C_J and charges q_i^g on the capacitances to the ground C_0 . Conservation of charge requires

$$2en_i - f_i - q_i^g + q_{i-1} - q_i = 0, \quad (\text{A1})$$

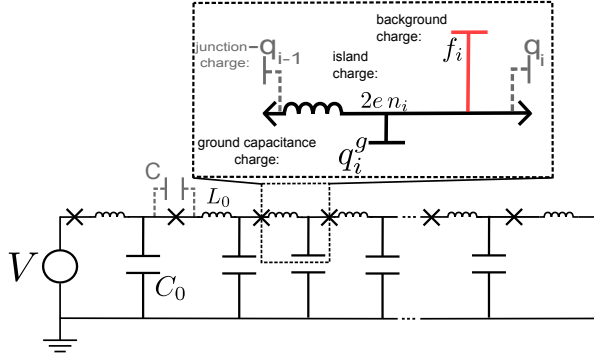


FIG. 3. (color online) Sketch of the Josephson junction array with inductances L_0 . The magnified part shows the distribution of the charges q_i^g , q_i , $2en_i$ and f_i on the island and the capacitances. In the language of electrical circuits the background charge f_i is given by the constant charge on an additional capacitance that is connected to the island, as shown in red in the magnified sketch of the island above.

where f_i are the random offset charges. Introducing the integrated charge variables $m_i \equiv \sum_{j=1}^i n_j$, $Q_i = 2e \sum_{j=1}^i q_j^g$, and $F_i = 2e \sum_{j=1}^i f_j$ one can easily obtain the following hamiltonian

$$H = \sum_{i=1}^N \left[\frac{1}{2C_J} (2em_i - F_i - Q_i)^2 - E_J \cos \phi_i + \frac{1}{2C_0} (Q_i - Q_{i+1})^2 + \frac{1}{2L_0} \Phi_i^2 \right], \quad (\text{A2})$$

where Φ_i is the flux on the inductance L_0 of the i -th island whereas ϕ_i is the phase drop on the i -th Josephson junction. The pairs of canonically conjugated variables in (A2) are (Q_i, Φ_i) and (m_i, ϕ_i) . The physical meaning of Q_i is clarified by the following relation

$$q_i = Q_i + F_i - 2em_i, \quad (\text{A3})$$

which can be obtained using (A1). The charge on the junction capacitance q_i is given by the total charge that has flown into the junction $Q_i + F_i$ minus the discrete charge $2em_i$ that has tunneled through the junction. As F_i is a constant offset charge, we understand that Q_i is the integral of current that has flown into the junction.

In Ref. 6 the inductance L_0 was assumed to be large, so that the dynamics of (Q_i, Φ_i) is adiabatic. In the current paper we assume $L_0 \rightarrow 0$ and claim that the emerging Bloch inductance, the large screening length Λ and the pinning disorder render an adiabatic regime in the vicinity of the depinning point.

Appendix B: Relation to Luttinger liquid

In the limit $E_J \gg E_C$ the Bloch inductance L_B approaches^{11,12} the Josephson inductance $L_J \equiv (\Phi_0/(2\pi))^2 E_J^{-1}$, whereas $U[Q] \approx -E_S \cos[2\pi Q/(2e)]$.

Here E_S is the exponentially small phase slip amplitude^{16,17}. Introducing $q_k = \pi Q_k/(2e)$ we obtain from Eq. (4) the discretized Lagrangian of the Luttinger liquid²⁸ with phase disorder in the backscattering term

$$\mathcal{L} = \frac{1}{2\pi K} \sum_k \left[\frac{\dot{q}_k^2}{v} - v (q_k - q_{k+1})^2 \right] + \sum_k E_S \cos[2q_k + \pi F_k/e]. \quad (\text{B1})$$

Here $v \equiv 1/\sqrt{L_J C_0}$ and $K \equiv \pi \sqrt{E_J/(8E_{C0})}$. Thus, for $F_k = 0$, i.e., without disorder, we reproduce the conclusions of Refs. 16 and 17. In the limit $\Lambda \rightarrow \infty$ we obtain $K \rightarrow 0$ and the relevant physics in the thermodynamic limit is that of classical pinning^{28,29}. Yet, since in the limit $E_J \gg E_C$ the pinning potential $\sim E_S$ is exponentially weak, systems of finite length may conduct or even be superconducting¹⁷.

Appendix C: Voltage bias at the edge

We consider the potential energy part of the Hamiltonian of the Josephson junction array,

$$H_C = \sum_i \left[\frac{(Q_i - Q_{i+1})^2}{2C_0} + U[Q_i + F_i] \right] - Q_{i=1} V. \quad (\text{C1})$$

Here the last term has been added to describe the voltage bias V applied on the left edge of the array. To transform an edge voltage bias to a homogeneous electric field we perform the following transformations $\tilde{Q}_i \equiv Q_i - A_i$ and $\tilde{F}_i \equiv F_i + A_i$, where $A_i \equiv C_0 V(N+1-i)(N-i)/2N$ and N is the length of the array. This gives

$$H_C = \sum_i \left[\frac{(\tilde{Q}_i - \tilde{Q}_{i+1})^2}{2C_0} + U[\tilde{Q}_i + \tilde{F}_i] - E \tilde{Q}_i \right], \quad (\text{C2})$$

where $E \equiv V/N$ is the homogeneous depinning force (electric field). In the case of maximal disorder the shift of the quasi-charge to include the voltages applied at the boundaries does not change the distribution function of the random charge \tilde{F}_i . Thus we can omit the tildes and we obtain the model of Eq.5. This property of the maximally disordered model is also referred to as statistic tilt symmetry³⁰.

Appendix D: The strength of the pinning potential

The strength of the pinning potential R can be obtained by numerically diagonalizing the single junction

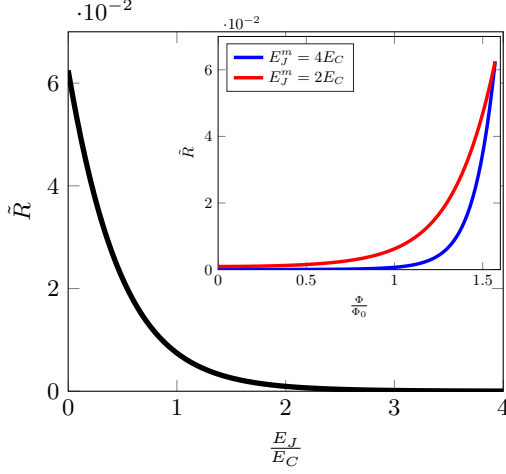


FIG. 4. (color online) The dimensionless strength of the pinning potential \tilde{R} as a function of E_J/E_C in the main plot and as a function of the magnetic flux Φ in the inset plot.

Hamiltonian

$$H(Q) = 4E_C \left(\left(\hat{m} - \frac{Q}{2e} \right)^2 + \frac{E_J}{8E_C} (|m+1\rangle \langle m| + \text{h.c.}) \right) \quad (\text{D1})$$

for a dense set of Q -values in the interval $[-e, e]$. For diagonalisation we use 15 charge state $|m\rangle$ with lowest charging energy. Including more states does not change the ground state energy $E_Q(Q)$ within our level of numerical accuracy. The value of the function \tilde{R} for each fixed value of E_J/E_C can be obtained by determining the amplitude of the periodic function $E_Q(Q)$. The result is shown in Fig. 4.

Appendix E: Switching voltage as a function of Josephson coupling energy

One of the dominant effects visible in Fig. 2 is the periodicity of the switching voltage V_{sw} with magnetic flux. This periodicity is a consequence of the periodicity of the Josephson coupling energy $E_J \propto \cos(\frac{\pi\Phi}{\Phi_0})$. The switching voltage V_{sw} is plotted as a function of E_J in Fig. 5.

Appendix F: Distribution of the switching voltage

The switching voltage V_{sw} shows strong fluctuations. The data presented in Fig. 2 are extracted from individual measurements of I/V characteristics. The bias voltage was ramped up once and the current response was detected by a transimpedance amplifier. In these measurement switching can easily be identified as evident from the sample IV-curve given in Fig. 1. The fluctuation in V_{sw} can be noticed from the apparent noise visible

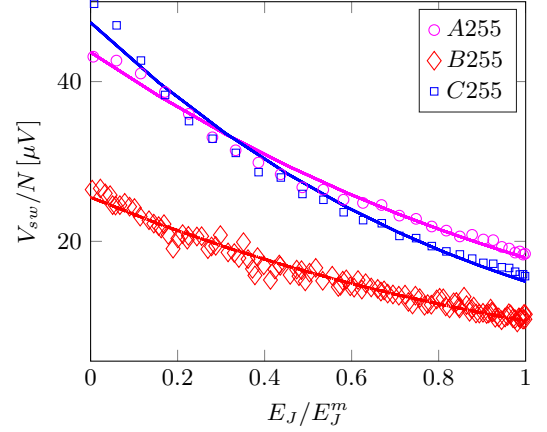


FIG. 5. (color online) The switching voltage as a function of E_J for arrays A255 (magenta), B255 (red) and C255 (blue).

in Fig. 2. For the sample B255 we have recorded many switching events at various fixed values of Φ and constructed histograms. The result of these measurements is summarized in Fig. 6, where the properties of histograms are visualized by red symbols and single switching events extracted from individual I/V characteristics are shown as blue dots. The latter data are the same as displayed in Fig. 2. Histograms are constructed from at least 10000 switching events. The events are sorted according to its switching voltage V_{sw} and the range of V_{sw} is divided in about 250 to 300 bins. To construct histograms, the events corresponding to each bin are counted. The mean V_{mean} of the histograms (this is 50 % of times the switching occurs at voltages lower than V_{mean}) is represented as red dots in Fig. 6. The red squares correspond to the voltage of the lowest bin containing at least 0.15 % of the events, the red diamonds to the highest bin containing at most 0.15 % of the event. The vertical distance between the squares and diamonds represent thus the full width of the histograms. Single events as seen in I/V characteristics (blue dots) fall well into the span of switching voltages recorded in a quite different manner for the purpose to construct the histograms.

The method to record a great number of events is rather conventional. A sawtooth like voltage signal with $0 < V < V_{max}$ has been applied as bias to sample B255 where V_{max} is considerable larger than the maximally observed switching voltage. Each time the bias starts to ramp at $V = 0$ a timer is started. The voltage output V_o of a transimpedance amplifier is used as a trigger signal to stop the timer as soon as V_o exceeds a threshold signaling that switching from a zero current to a finite current state has occurred. Retrapping occurs when the bias is set back to zero at the end of each voltage ramp. The time span between start and stop trigger is a measure of the switching voltage of a single event. The frequency of the sawtooth signal is of the order of 20 Hz and the recording of a histogram takes about 10 minutes.

The current needs to be detected with a relative large

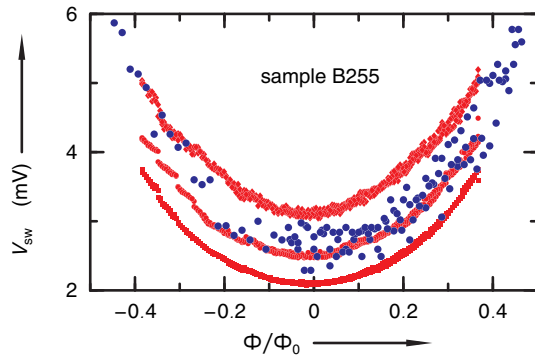


FIG. 6. (color online) Comparison of switching voltage extracted from single sweeps (blue dots) and full switching voltage histograms (red symbols). The data displayed in red show the width of the histograms (see text for an explanation).

bandwidth. The resolution of the current measurement is for this reason considerable worse than the resolution achieved in measurements of individual I/V characteristics. In the latter case the bias voltage can be varied very slowly while the output of the transimpedance amplifier is averaged to yield the desired current resolution. To construct a histogram many events have to be measured and a histogram can be constructed in a reasonable time only when the current after switching is sufficiently large to be detected quickly. Since the current after switching is getting smaller close to full frustration $\Phi = (n+1/2)\Phi_0$ histograms could only be measured in the range of small frustrations depicted in Fig. 6

- ¹ D. B. Haviland, K. Andersson, and P. Ågren, J. Low Temp. Phys. **118**, 733 (2000).
- ² A. Ergül, D. Schaeffer, M. Lindblom, D. B. Haviland, J. Lidmar, and J. Johansson, Phys. Rev. B **88**, 104501 (2013).
- ³ A. Ergül, J. Lidmar, J. Johansson, Y. Azizoğlu, D. Schaeffer, and D. B. Haviland, New Journal of Physics **15**, 095014 (2013).
- ⁴ J. Zimmer, N. Vogt, A. Fiebig, S. V. Syzranov, A. Lukashenko, R. Schäfer, H. Rotzinger, A. Shnirman, M. Marthaler, and A. V. Ustinov, Phys. Rev. B **88**, 144506 (2013).
- ⁵ E. Ben-Jacob, K. Mullen, and M. Amman, Physics Letters A **135**, 390 (1989).
- ⁶ Z. Hermon, E. Ben-Jacob, and G. Schön, Phys. Rev. B **54**, 1234 (1996).
- ⁷ D. B. Haviland and P. Delsing, Phys. Rev. B **54**, R6857 (1996).
- ⁸ P. Ågren, K. Andersson, and D. B. Haviland, J. Low Temp. Phys. **124**, 291 (2001).
- ⁹ S. Brazovskii and T. Nattermann, Advances in Physics **53**, 177 (2004).
- ¹⁰ V. Gurarie and A. M. Tsvelik, J. Low Temp. Phys. **135**, 245 (2004).
- ¹¹ J. Homfeld, I. Protopopov, S. Rachel, and A. Shnirman, Phys. Rev. B **83**, 064517 (2011).
- ¹² A. B. Zorin, Physical Review Letters **96**, 167001 (2006).
- ¹³ R. Schäfer, W. Cui, K. Grube, H. Rotzinger, and A. V. Ustinov, “Dissipation mechanism above the current threshold in Josephson junction chains,” (2013), arXiv:1310.4295.
- ¹⁴ A. A. Middleton and N. S. Wingreen, Physical Review Letters **71**, 3198 (1993).
- ¹⁵ J. Johansson and D. B. Haviland, Phys. Rev. B **63**, 014201 (2000).
- ¹⁶ S. E. Korshunov, Sov. Phys.-JETP **68**, 609 (1989).
- ¹⁷ G. Rastelli, I. M. Pop, and F. W. J. Hekking, Phys. Rev. B **87**, 174513 (2013).
- ¹⁸ M.-S. Choi, J. Yi, M. Y. Choi, J. Choi, and S.-I. Lee, Phys. Rev. B **57**, R716 (1998).
- ¹⁹ A. I. Larkin, Sov. Phys. JETP **31**, 784 (1970).
- ²⁰ Y. Imry and S.-k. Ma, Physical Review Letters **35**, 1399 (1975).
- ²¹ H. Fukuyama and P. A. Lee, Phys. Rev. B **17**, 535 (1978).
- ²² E_p corresponds here to the depinning force f_p in the notations of Ref. 9. This estimate can be improved with the help of an RG treatment^{9,31,32}. The improved estimate is called f_c in Ref. 9. The relevance of this RG procedure in our case is questionable since our arrays are not much longer than Larkin length.
- ²³ K. G. Fedorov, M. V. Fistul, and A. V. Ustinov, Phys. Rev. B **84** (2011), 10.1103/PhysRevB.84.014526.
- ²⁴ M. V. Feigel'man, Sov. Phys. JETP **52**, 555 (1980).
- ²⁵ I. L. Aleiner and I. M. Ruzin, Physical Review Letters **72**, 1056 (1994).
- ²⁶ M. M. Fogler, Physical Review Letters **88**, 186402 (2002).
- ²⁷ J. H. Cole, J. Leppäkangas, and M. Marthaler, New Journal of Physics **16**, 063019 (2014).
- ²⁸ T. Giamarchi, *Quantum Physics in One Dimension*, International Series of Monographs on Physics (Clarendon Press, 2003).
- ²⁹ A. D. Mirlin, D. G. Polyakov, and V. M. Vinokur, Phys. Rev. Lett. **99**, 156405 (2007).
- ³⁰ A. A. Fedorenko, P. Le Doussal, and K. J. Wiese, Phys. Rev. E **74**, 061109 (2006).
- ³¹ P. Chauve, T. Giamarchi, and P. Le Doussal, Phys. Rev. B **62**, 6241 (2000).
- ³² P. Chauve, P. Le Doussal, and K. J. Wiese, Physical Review Letters **86**, 1785 (2001).